Front. Med. 2024, 18(1): 128−146
https://doi.org/10.1007/s11684-023-1010-1

RESEARCH ARTICLE

Tumor-derived exosomes induce initial activation by exosomal CD19 antigen but impair the function of CD19-specific CAR T-cells via TGF-β signaling

Yuanyuan Hao[1,2,*], Panpan Chen[1,*], Shanshan Guo[1,*], Mengyuan Li[1], Xueli Jin[1], Minghuan Zhang[1], Wenhai Deng[3], Ping Li[4], Wen Lei (✉)[1], Aibin Liang (✉)[4], Wenbin Qian (✉)[1]

[1]Department of Hematology, The Second Affiliated Hospital, College of Medicine, Zhejiang University, Hangzhou 310009, China; [2]Department of Hematology, Henan Provincial People's Hospital; Zhengzhou University People's Hospital, Zhengzhou 450003, China; [3]Key Laboratory of Laboratory Medicine, Ministry of Education, School of Laboratory Medicine and Life Sciences, Wenzhou Medical University, Wenzhou 325000, China; [4]Department of Hematology, Tongji Hospital of Tongji University, Shanghai 200065, China

Abstract **Tumor-derived exosomes (TEXs) enriched in immune suppressive molecules predominantly drive T-cell dysfunction and impair antitumor immunity. Chimeric antigen receptor (CAR) T-cell therapy has emerged as a promising treatment for refractory and relapsed hematological malignancies, but whether lymphoma TEXs have the same impact on CAR T-cell remains unclear. Here, we demonstrated that B-cell lymphoma-derived exosomes induce the initial activation of CD19–CAR T-cells upon stimulation with exosomal CD19. However, lymphoma TEXs might subsequently induce CAR T-cell apoptosis and impair the tumor cytotoxicity of the cells because of the upregulated expression of the inhibitory receptors PD-1, TIM3, and LAG3 upon prolonged exposure. Similar results were observed in the CAR T-cells exposed to plasma exosomes from patients with lymphoma. More importantly, single-cell RNA sequencing revealed that CAR T-cells typically showed differentiated phenotypes and regulatory T-cell (Treg) phenotype conversion. By blocking transforming growth factor β (TGF-β)–Smad3 signaling with TGF-β inhibitor LY2109761, the negative effects of TEXs on Treg conversion, terminal differentiation, and immune checkpoint expression were rescued. Collectively, although TEXs lead to the initial activation of CAR T-cells, the effect of TEXs suppressed CAR T-cells, which can be rescued by LY2109761. A treatment regimen combining CAR T-cell therapy and TGF-β inhibitors might be a novel therapeutic strategy for refractory and relapsed B-cell lymphoma.**

Keywords tumor-derived exosome; chimeric antigen receptor T-cell; lymphoma; TGF-β

Introduction

CD19-specific chimeric antigen receptor (CAR) T-cell therapy is remarkably effective in treating patients with B-cell malignancies, particularly those who are refractory to traditional cancer treatment modalities [1,2]. Unfortunately, a substantial number of patients achieving remission at the beginning of CAR T-cell treatment will show relapse subsequently due to CAR T-cell malfunction and short persistence *in vivo* or altered target antigen expression, which is a well-recognized phenomenon in lymphoma and leukemia, on tumor cell surfaces [3,4]. In recent years, many investigators, including our team, have attempted to adopt novel strategies to overcome CAR T-cell therapy resistance by targeting multiple tumor antigens [5–8], decreasing T-cell exhaustion via the blockage of the PD-1–PD-L1 immune checkpoint pathway [9], and sensitizing tumor cells to CAR T-cell-mediated cell death with various genetic engineering approaches [10]. However, the majority of patients with refractory and relapsed lymphoma and leukemia have shown no response or have shown eventual tumor recurrence after CAR T-cell infusion, suggesting that an unknown mechanism underlies resistance to this novel therapeutic modality.

Received November 29, 2022; accepted May 19, 2023

Correspondence: Wenbin Qian, qianwb@zju.edu.cn;
Aibin Liang, lab7182@tongji.edu.cn;
Wen Lei, leiwen2017@zju.edu.cn

*Yuanyuan Hao, Panpan Chen, and Shanshan Guo contributed equally to this study.

Found in all body fluids, exosomes are nanoscale (30–150 nm) extracellular vesicles produced virtually by normal and pathological cells [11]. The exosome-mediated intercellular transfer of proteins, RNA, DNA, transcription factors, lipids, and other biologically active constituents confers physiologic and pathological functions on recipient cells [11–14]. Compared with normal cells, tumor cells produce considerable amounts of exosomes and tumor-derived exosomes (TEXs) [15,16]. TEXs are implicated in tumorigenesis and tumor metastasis through diverse mechanisms, including transfer of oncogenic molecules to recipient cells, suppression of immune cell function, promotion of regulatory T-cell (Treg) expansion, and tumor-supportive microenvironment formation [17–19].

T-cell dysfunction plays an important role in the ability of tumors to escape immune surveillance. Although having immunostimulatory effects on T-cells under some circumstances, TEXs can carry a variety of immune suppressive molecules predominantly driving T-cell dysfunction and impairing tumor immunity [12,20]. Exosomes produced by cancer cell lines or isolated from the sera of patients with cancer suppress T lymphocyte proliferation and cytotoxicity, inhibit Th1 and Th17 differentiation, promote Treg expansion, and induce T-cell apoptosis and exhaustion [20,21]. However, little information is known regarding the effect of TEXs on CAR T-cells.

In the current study, we characterized the effects of TEXs derived from B-cell malignant cell lines on CD19-specific CAR T-cells and found that TEX exposure positively regulated CAR T-cell cytotoxic function upon exosomal CD19 stimulation. However, we found that priming with Raji TEXs, which contains CD19, upregulated the expression of immune checkpoints, including PD-1, TIM3, and LAG3, in the CAR T-cells and subsequently induced a differentiated phenotype evidenced by increases in T effector cells (T_{EFF}) and decreases in T central memory cells (T_{CM}) and naïve T-cells ($T_{Naïve}$). These dual effects were observed in the CAR T-cells cocultured with plasma exosomes from patients with lymphoma. Moreover, data from single-cell RNA sequencing (scRNA-seq) further revealed that the gene expression levels of the specific markers of T_{CM} and $T_{Naïve}$ cells, such as interleukin (IL) 7 receptor, LEF1, SELL, and JUNB, were downregulated considerably in TEX-primed CAR T-cells. Importantly, we demonstrated that exosomal transforming growth factor (TGF)-β of lymphoma cells impaired the function of CAR T-cells by inducing cell apoptosis, upregulating immune checkpoints, and subsequently resulting in terminally differentiated phenotype and Treg conversion. Furthermore, the blockade of TGF-β signaling with the small-molecule inhibitor LY2109761 enhanced the tumor-elimination efficacy of CD19-specific CAR T-cells.

Materials and methods

Cell lines and reagents

The Burkitt lymphoma cell line Raji and acute lymphoblastic leukemia cell line Nalm-6 were purchased from the American Type Culture Collection (ATCC; Manassas, VA, USA). The human DLBCL (non-GCB) cell line OCI-LY3 was preserved in our laboratory, and short tandem repeat profiling revealed that the cell line was well above the 90% match threshold. Raji and Nalm-6 cells were cultured in RPMI 1640 medium supplemented with 10% fetal bovine serum (FBS, Gibco, USA), 1% penicillin–streptomycin solution (Gibco), and 1% glutamine (Gibco). The OCI-LY3 cells were cultured in Iscove's modified Dulbecco's medium containing 20% FBS, 1% penicillin–streptomycin solution, and 1% glutamine. Non-exosomal components containing FBS were obtained by ultracentrifugation at 100 000 *g* for 18 h to remove possible FBS-containing exosomes before use. Raji–Luc-enhanced green fluorescent protein (EGFP) cells were constructed through lentiviral transduction for the expression of the EGFP-firefly luciferase fusion gene. The cells were then subjected to single-cell clone and fluorescence-activated cell sorting, and CD19-knockout (KO) Raji cells were generated by CRISPR–Cas9-mediated gene KO according to previously described method [6]. The TGF-β inhibitor LY2109761 was purchased from MedChemExpress (New Jersey, USA).

Isolation of extracellular vesicles

To obtain extracellular vesicles released from OCI-LY3, Raji, and Nalm-6 cells, we cultured the cells for 48 h in a complete medium. The supernatants were collected, sequentially centrifuged at 500× *g* for 5 min and then at 2000× *g* for 10 min, and filtered for the removal of cellular debris with 0.45 and 0.22 μm filters (Millipore, Bedford, MA, USA). Then, the supernatant was subjected to ultracentrifugation at 100 000× *g* for 70 min at 4 °C and washed with phosphate-buffered saline (PBS) and ultracentrifuged at 120 000× *g* for 70 min. Finally, the pelleted extracellular vesicles were resuspended in PBS and stored at −80 °C until usage. The plasma samples of 18 patients with B-cell malignancy were filtered to exclude particles large than 0.22 μm, and exosomes were extracted using an exosome isolation and purification kit (MedChemExpress) according to the manufacturer's protocol.

Transmission electron microscopy (TEM)

TEXs were loaded onto the bright side of a copper grid and stained with 2% uranyl acetate for 5 min at room temperature (RT). Next, excess solution was removed by

filter paper, and the grid was observed by TEM (JEM-1200EX, JEOL, Japan).

Characterizations of exosomes

The quality of exosomes was confirmed by dynamic light scattering (DLS) by using a particle and molecular size analyzer (Zetasizer 3000, Malvern, USA) according to the manufacturer's instructions. The concentration of exosomes was determined with a BCA assay (Sigma-Aldrich, USA) for the measurement of total protein.

Phenotypic characterization of exosomes

Approximately 30 μg of exosomes were precoated with 10 μL of aldehyde/sulfate latex beads (Invitrogen, Carlsbad, CA, USA) overnight at RT and stopped by 0.1% bovine serum albumin. Then, the exosomes were stained with FITC-labeled CD19 (clone HIB19), PE-labeled CD20 (clone 2H7), APC-labeled PD-L1 (clone 29E.2A3), and their corresponding isotype-matched antibodies (clone MOPC-173) for 30 min at 4 °C in the dark. Flow cytometry analysis was then performed (ACEA, Agilent, Santa Clara, CA, USA). All these antibodies were obtained from Biolegend (CA, USA).

Western blot analysis

Western blots were performed as described previously [20]. In brief, the exosome and cell samples were collected and washed twice with PBS and then lysed in RIPA buffer (Cell Signaling Technology, USA), including 1 mmol/L PMSF (Cell Signaling Technology) for 30 min on ice. The cell lysates were collected through centrifugation at 13 000× *g* at 4 °C for 15 min, and protein concentrations were calculated using a BCA protein assay kit. Protein samples were separated by SDS-polyacrylamide gel electrophoresis and then electroblotted onto PVDF membranes. The membranes were blocked in 5% nonfat milk for 1 h and incubated with primary antibodies at 4 °C overnight. The membranes were washed and incubated with a secondary antibody conjugated with horseradish peroxidase. An ECL-detecting kit (Thermo Fisher, USA) was applied to visualize results. The following antibodies were used for Immublot: rabbit anti-CD63 (clone EPR5702, dilution 1:1000), anti-ALIX (clone EPR15314-33, dilution 1:1000), anti-TSG101 (clone EPR7130(B), dilution 1:1000), anti-cytochrome C (clone EPR1327, dilution 1:1000), anti-HSP70 (clone EPR16892, dilution 1:1000), anti-Rab27a (clone D7Z9Q, dilution 1:1000), anti-GAPDH (clone ^{14}C10, dilution 1:1000), anti-TGF-β (clone ERP18163, dilution 1:1000), anti-CD19 (clone ERP5906, dilution 1:1000), anti-Smad3 (clone 4D3, dilution 1:1000), anti-phosphorylated Smad3 (clone S423/S425, dilution 1:1000), anti-Flag (M2, dilution 1:1000), and mouse anti-β-actin (clone mAbcam 8226, dilution 1:1000). Most antibodies were obtained from Abcam (USA), except anti-Rab27a and anti-GAPDH from Cell Signaling Technologies, anti-Smad3 and phosphorylated Smad3 from HUABI (Hangzhou, China), and anti-Flag from Sigma. The following secondary antibodies were used: HRP-conjugated goat anti-rabbit IgG Goat polyclonal antibody (dilution 1:5000; HUABIO) and HRP-conjugated goat anti-mouse IgG goat polyclonal antibody (dilution 1:5000; HUABIO). Protein bands were detected using a Pierce ECL Western blotting substrate (ThermoFisher) in a multi-automatic chemiluminescence–fluorescence image analysis system (Tanon 5200 Multi, Shanghai).

Real-time PCR of FOXP3

Total RNA was collected by an RNA-quick purification kit (Esunbio, Hangzhou, China) and then used in a reverse transcriptase reaction with a PrimeScript RT reagent kit (Takara, Kyoto, Japan). TB Green Premix Ex Taq kit (Takara) was used for the thermocycling reaction in an ABI-7500 fast real-time PCR system (Thermo Scientific). qPCR analysis was carried out in triplicate with the following primer sets: FOXP3 (forward: 5′-CACTGCCCCTAGTCATGGTG-3′; Reverse: 5′-GGTG-CATGAAATGTGGCCTG-3′).

Lentiviral vector and CAR T-cell production

The CD19–CAR lentivirus vector used in this study is a classical second generation of anti-human CD19–CAR, which contains an scFv FMC63-based targeting domain, CD8-derived hinge region, trans-membrane domain, 41BB/CD137 costimulatory domain, and CD3ζ chain intracellular signal domain. The CAR fragment was promoted by EF1a promoter.

Peripheral blood mononuclear cells were isolated from peripheral blood of healthy donors using Ficoll-Paque density gradient centrifugation, following activation for 24 h with anti-CD3/CD28 Dynabeads (Thermo Fisher). The activated T-cells were transduced with CD19–CAR lentivirus at the indicated dose on day 2. The transfected efficiency was determined using an Alexa Fluor 647-anti-mouse FMC63 scFv monoclonal antibody (mAb; R19M, dilution 1:200), followed by purified by FACS (BD FACSAria III, USA) sorting to ⩾ 98% purity on day 4. The purified CD19–CAR$^+$ T-cells were expanded for additional 9–11 days in the complete AIM-V medium (Gibco) supplemented with 10% FBS (Gibco), IL-2 (300 IU/mL, PeproTech, USA), IL-7, and IL-15 (5 ng/mL, Novoprotein, China). Matured CAR T-cells were used immediately or cryopreserved in liquid nitrogen for future use.

Confocal laser scanning microscopy

The interaction between exosome and CAR T-cells was visualized via confocal laser scanning microscopy. In detail, CAR T-cells were stained with 1 μg/mL Hoechst 33258 (Sigma) at 37 °C for 20 min to mark the nuclear localization and then incubated in 200 μL of complete medium with 20 μg of PKH67 (Sigma)-labeled exosomes for 6 h. The internalization of exosomes by CAR T-cells was observed under a confocal microscope (Carl Zeiss, German).

CAR T-cell cytotoxicity assays

To determine the TEX-pretreated or untreated CAR T-cells mediated cytotoxicity, luciferase-based cytotoxicity assays were performed as described previously [9]. Target tumor cells Raji–Luc–EGFP, stably transduced with firefly luciferase, were constructed in our laboratory. Then, 5×10^3 tumor cells were cultured with TEX-pretreated or untreated CAR T-cells at indicated effector-to-target ratios for 4 h in 96-well plates. D-Luciferin potassium salt (0.5 mM; PerkinElmer, USA) was added to each well, and the resulting luminescence was analyzed on a multimode reader (SpectraMax i3, USA) with 1000 ms/well. Target and target-only cells plus 2.5% X-triton 100 (Sigma) were used as Max luminescence and Min luminescence for determining the assay range. The specific cytotoxicity was calculated using the following formulas: cytotoxicity (%) = $(OD_{Max} - OD_{Sample})/(OD_{Max} - OD_{Min}) \times 100\%$. Each experiment was repeated at least three times.

Flow cytometry analysis

CAR T-cells were cultured at a density of 1×10^6 cells/mL in a 96-well plate and treated with TEXs (100 μg/mL) for 48 h and then were collected and washed twice with PBS containing 2% FBS. Surface staining was performed for 30 min at 4 °C with FITC-conjugated CD4 (clone OKT4), PE-conjugated CD8 (clone RPA-T8), PE-Cy7-conjugated CD45RA (clone HI100), Percp-Cy5.5-conjugated CD62L (clone DREG-56), PE-Cy7-conjugated CD25 (clone BC96), and APC-conjugated CD69 (clone FN50). FITC-conjugated Tim-3 (F38-2E2), PE-conjugated LAG3 (clone 11C3C65), and PE-Cy7-conjugated PD-1 (clone EH12.1). For the intracellular staining of Ki-67, FOXP3, and granzyme B, Alexa Fluor 488-conjugated Ki-67 (clone Ki-67) and APC-conjugated granzyme B (clone QA16A02) were stained after surface staining and fixation and permeabilization with a fixation buffer (Cat#420801) and intracellular staining permeabilization wash buffer (Cat#421002) according to the manufacturer's instructions. Flow cytometric data were acquired with a NovoCyte flow cytometer (ACEA Biosciences, Inc, San Diego, California, USA). All the antibodies and regent buffers were obtained from Biolegend except PE/Cy7-conjugated anti-human PD-1 from BD Biosciences.

The subtypes of CAR T-cells were described as T_{CM} ($CD45RA^-CD62L^+$), $T_{Naïve}$ ($CD45RA^+CD62L^+$), T_{EFF} ($CD45RA^+CD62L^-$), and T_{EM} ($CD45RA^-CD62L^-$), $CD4^+$ and $CD8^+$ T-cells. PE–Cy7-conjugated CD25 and APC-conjugated CD69 were used to define the activation of CAR T-cells. FITC-conjugated Tim-3, PE-conjugated LAG3, and PE-Cy7-conjugated PD-1 were defined as the immunosuppressive receptors on the CAR T-cells. Tregs were analyzed as $CD4^+$ $CD25^+$ $Foxp3^+$ subtypes.

Cytokine release assay

For the cytokine release assays, CAR T-cells were cocultured with Raji–Exo or OCI-LY3–Exo at 100 μg/mL for 48 h. Harvested supernatants were analyzed for secreted cytokines, such as IL-4, IL-6, IL-10, TNF-α, and IFN-γ, with a cytometric bead array human Th1/Th2 cytokine kit (BD, USA). Data were acquired with a NovoCyte flow cytometer and analyzed by the ACP Array v3.0.1.

CAR T-cell proliferation assay

CAR T-cells were labeled with carboxyfluorescein succinimidyl ester (CFSE, Invitrogen) as previously described [20]. Briefly, CAR T-cells (1×10^6 cells) were stained with 1 μmol/L CFSE dye at 37 °C in the dark for 30 min and then treated with TEXs (100 μg/mL) for 48 h. The dilution of CFSE was evaluated by flow cytometry analysis.

Cell cycle analysis

Cell cycle staining kit (Dawenbio, Hangzhou, China) was used for cell cycle analysis according to the manufacturer's instructions. In brief, CAR T-cells were treated with TEXs (100 μg/mL) for 48 h and were collected and washed twice with cold PBS. Then, the cells were incubated with 1 mL of DNA staining solution and 10 μL of permeabilization solution for 30 min at RT in dark. Data were collected and analyzed with NovoCyte flow cytometer.

CRISPR-Cas9-mediated KO of *Rab27a*

The genomic guide RNA *Rab27a* target sequences were 5′-CCAAAGCTAAAAACTTGATG-3′, as mentioned by Poggio *et al*. [22]. The process of CRISPR-Cas9-mediated KO consisted of the lentivirus packaging of Lenti-guide puro or Lenti-cas9-blast and a single-cell

cloning screen, as described by Lin *et al*. [23]. Guide RNA for *Rab27a* synthesis and the construct of Lenti-g*Rab27a* puro or Lenti-cas9-blast vectors were accomplished by Micro-helix Co, LTD (Beijing, China).

For Lenti-g*Rab27a* puro or Lenti-cas9-blast lentivirus production, 293T/17 (CRL-11268, ATCC) cells were transfected with Lenti-g*Rab27a* puro vector or Lenti-cas9-blast vector, psPAX2 (HIV-1 gag pol-expressing plasmid), and pMD2.G (VSV-G envelope-expressing plasmid) in a ratio of 4:1:2 by using a Neofect DNA transfection reagent (Neofect, Beijing) and cultured in Dulbecco's modified eagle medium (DMEM, Gibco) supplemented with 10% FBS and 1% penicillin/streptomycin. The virus supernatant was harvested from the culture medium after 48 and 72 h, and cell debris were separated using a 0.45 μm filter (Millipore). The virus suspension was concentrated through centrifugation at 4000× *g* and 4 °C for 12 h, resuspended in 200 μL of DMEM medium, and stored at −80 °C.

For *Rab27a* KO cell line construction, Raji cells (CCL-86, ATCC) underwent two-step lentivirus transduction. First, 50 multiplicity of infection of Lenti-cas9-blast lentivirus-infected Raji cells were incubated for 10 h and then subjected to blasticidin (20 μg/mL) treatment for the production of Cas9–blast-positive cells. The success of Cas9–blast lentivirus transfection was ascertained by the immunoblot of Flag expression. Second, Cas9–blast-positive Raji cells were re-transduced with Lenti-g*Rab27a* puro lentivirus for 10 h, and *Rab27a* KO–positive cells by puromycin (2 μg/mL) and blasticidin (20 μg/mL). Single-cell cloning was selected for 7–10 days before colony formation. The cells in the 96-well plate were collected, which only contained one colony, and then expanded in a 24-wells plate for 3 days. Cell lysates were collected, and *Rab27a* KO was confirmed through Western blot using *Rab27a* antibody.

Cell viability assays

Cell viability was monitored with 3-(4,5-dimethylthiazol-2-yl)-2,5-diphenyltetrazolium bromide (MTT; Sigma) assay. Briefly, CAR T-cells (1×10^5 cells/well) were seeded in 96-well plates and treated with TEXs at indicated doses. After 6 h of incubation, 20 μL of MTT solution (5 mg/mL) was added to each well, and the samples were then incubated at 37 °C for 4 h. Lysis buffer (10% SDS, 5% isobutanol, and 0.012 mol/L HCl) was added, and absorbance was measured at 570 nm after 16 h.

Animal experiments

All animal studies were performed with the approval of the institutional animal care and use committee of Zhejiang University and in compliance with the Chinese National Laboratory Animal Guideline for Ethical Review of Animal Welfare. Raji–*Rab27a* KO–GFP–luciferase cells (1×10^5/mouse) were injected into the lateral tail vein of 5 to 6-week-old female NOD SCID IL-2Rγ−/−(NSG) mice (#NM-NSG-001, Shanghai Model Organisms Center, Inc., Shanghai, China). Five days later, tumor engraftment was measured by i.p. injection of 150 mg/kg luciferin and imaging on a Xenogen IVIS-200 instrument (Caliper Biosciences, now Perkin Elmer, Shelton, Connecticut, USA). 1×10^6 Raji–Exo-pretreated CAR T-cells or untreated CAR T-cells were injected intravenously into every mouse on day 5. PBS-treated mice were included in the control group. Imaging was performed 1, 4, 12, 19, 26, 33, 40, 47, and 50 days after injection to establish the kinetics of tumor growth and eradication by CAR-T. Images were analyzed using Living Image (version 4.1; Perkin Elmer), and the bioluminescent signal flux for each mouse was expressed as total flux (P/S). The mice were euthanized by carbon dioxide inhalation upon hindlimb weakness or paralysis when necessary.

In the experiment where CD19–CAR T-cells were combined with TGF-β inhibitor for treatment *in vivo*, 1×10^5 Raji–Luc–EGFP cells were injected into NSG mice by intravenous injection for 7 days to establish the lymphoma xenograft model. After engraftment of Raji cells, mice were treated with vehicle, CAR T-cells (1×10^6 cells), or CAR T-cells combined with TGF-β inhibitor LY2109761. In combinational groups, LY2109761 was used orally on day 2 before CAR-T infusion at 50 mg/kg or 100 mg/kg twice a day and consistent for 5 days per week for 8 weeks from the day of CAR-T infusion. The tumor growth was monitored by bioluminescence imaging twice a week using the IVIS Lumina II *in vivo* imaging system, and the mice's survival was recorded every day.

Single-cell sorting RNA-seq for CAR-T samples (10x Genomics)

All experiments involving human subjects samples following the principles of the Declaration of Helsinki. ScRNA-seq samples were collected from the Raji–Exo primed CAR-T or untreated CAR-T from 3 patients. Single-cell suspensions of all samples were resuspended in PBS at 1×10^6 cells/mL. Then scRNA-seq libraries were generated using a Chromium Single-Cell 3′ Library and Gel Bead Kit (10x Genomics) using v3.1 for CAR T samples according to the manufacturer's protocol. For raw data processing and analysis, cells with fewer than 200 detected genes, greater than 6000 detected transcripts, or total mitochondrial gene expression exceeding 15% were excluded from the analysis. Genes expressed in less than three cells were also removed. Then, all the six scRNA-seq sample data were integrated

by using the Seurat (version 4.0.5) R package. The data were then normalized using the NormalizeData function in Seurat (LogNormalize method with a scale factor of 10 000). Anchors were identified using FindIntegration-Anchors with 1–60 dimensions and 5000 anchor features. Anchors were identified using FindIntegrationAnchors with 1–20 dimensions. Downstream analysis after integration included data feature scaling (ScaleData), principal component analysis (PCA; RunPCA), and shared nearest neighbor graph building (FindNeighbors). The first 30 dimensions were used for uniform manifold approximation and projection (UMAP) reduction with the RunUMAP function. Cells were clustered using the FindClusters function in Seurat at a resolution of 0.5. A total of 14 clusters were defined by common markers, and marker genes were identified using the FindAllMarkers function.

Statistical analysis

Differences between the TEX-exposed and untreated CAR T-cell groups were statistically analyzed by using SPSS 17.0. Student's *t*-test or two-way analysis of variance was analyzed, and significance was indicated by $P < 0.05$. Animal survival data were analyzed by log-rank analysis.

Results

Characterization and surface markers of exosomes from B-cell malignancies

The exosomes were isolated from Raji and OCI-LY3 cell lines with ultracentrifugation, and their sizes and surface zeta potentials were determined by using DLS. The mean surface zeta potentials of exosomes derived from Raji and OCI-LY3 were −19.9 and −10.4 mV, respectively. The size distributions of the two types of exosomes ranged from 28.7 ± 11.6 nm to 75.2 ± 6.2 nm (Fig. 1A), and the morphology of the exosomes examined by TEM showed a population with typical exosomal pellets (Fig. 1B). Additionally, Western blot analysis depicted the features of the exosomes, including proteins from the multivesicular body formation machinery (ALIX and TSG-101), tetraspanins (CD63), and heat shock protein HSP70 (Fig. 1C). Recent studies showed that CD20 on exosomes from B-cell lymphoma cells bound the therapeutic anti-CD20 antibody rituximab, suggesting that exosomal B-cell antigens might intercept immunotherapy [24,25]. We therefore examined the expression of B-cell antigens and PD-L1 on Raji, Nalm-6, and OCI-LY3 cell lines and their exosomes. The results showed that CD19 was detected in Raji and Nalm-6 TEXs derived from originating tumor host cells, whereas OCI-LY3 cells and derived exosomes did not show CD19 expression (Fig. 1D), suggesting the heterogeneity in exosomal CD19 molecule expression among the B-cell tumor cell lines.

We then analyzed the characterization of plasma exosomes harvested from the patients with B-cell lymphoma. The protein markers ALIX, TSG-101, and CD63 detected by using immunoblotting indicated successful extraction of exosomes. The plasma exsomes from 3/6 cases showed high levels of TGF-β (Fig. 1E). Analysis of plasma exosomes by Western blot and flow cytometry also revealed heterogeneity in exosomal CD19 expression (Fig. 1E and 1F).

Priming with CD19-containing lymphoma exosomes activates CD19-specific CAR T-cells

Exosomes can be internalized by various cell types although underlying mechanisms are not entirely understood [12,15]. To examine whether TEXs are internalized by CAR T-cells, CD19–CAR T-cells were sorted through flow cytometry (Fig. S1A) and then incubated with the fluorescent dye PKH67-labeled Raji or OCI-LY3 TEXs. Exosomal internalization in CAR T-cells was demonstrated by confocal microscopy at 6 h post-incubation (Fig. 2A), which was consistent with recent observation that lymphoma exosomes are assimilated by CAR T-cells within 4 h [26]. Thereafter, we explored whether TEXs influence the killing of B-cell tumor cells by CAR T-cells. First, CD19–CAR T-cells were cocultured with lymphoma cell-derived exosomes for 48 h. Then, the CAR T-cells were cocultured with Raji cells for 4 h after washing with PBS, and specific lysis was analyzed. The result indicated that CAR T-cells primed with Raji TEXs exhibited significantly increased cytolytic activity compared with those without Raji TEX priming. However, CAR T-cells primed with OCI-LY3 TEXs did not show any enhancement in cytotoxicity against Raji cells (Fig. 2B). The increases in multiple cytokines and granzyme B were the responses to CAR T-cell activation and cytotoxicity [27]. We found that Raji TEX–primed CD19–CAR T-cells produced higher levels of Th1 cytokines (TNF-α and IFN-γ) and Th2 cytokines, such as IL-4, IL-6, and IL-10 (Fig. 2C). Meanwhile, a significantly high level of granzyme B was observed only in the CAR T-cells treated with Raji TEXs (Fig. 2D). Furthermore, exosomes derived from Raji cells but not from OCI-LY3 cells significantly promoted the activation and proliferation of CAR T-cells *in vitro*, manifested as decreased proportion of cells diluted with CFSE dye and S phase entry, upregulation of Ki-67, and increased expression of early cell activation markers, including CD25 and CD69 (Fig. 2E). Similar results were observed in CAR T-cells primed with Nalm-6 TEXs containing CD19 antigen and those cocultured with plasma exosomes that expressed relatively high level of exosomal CD19 (Fig. S1B–S1D).

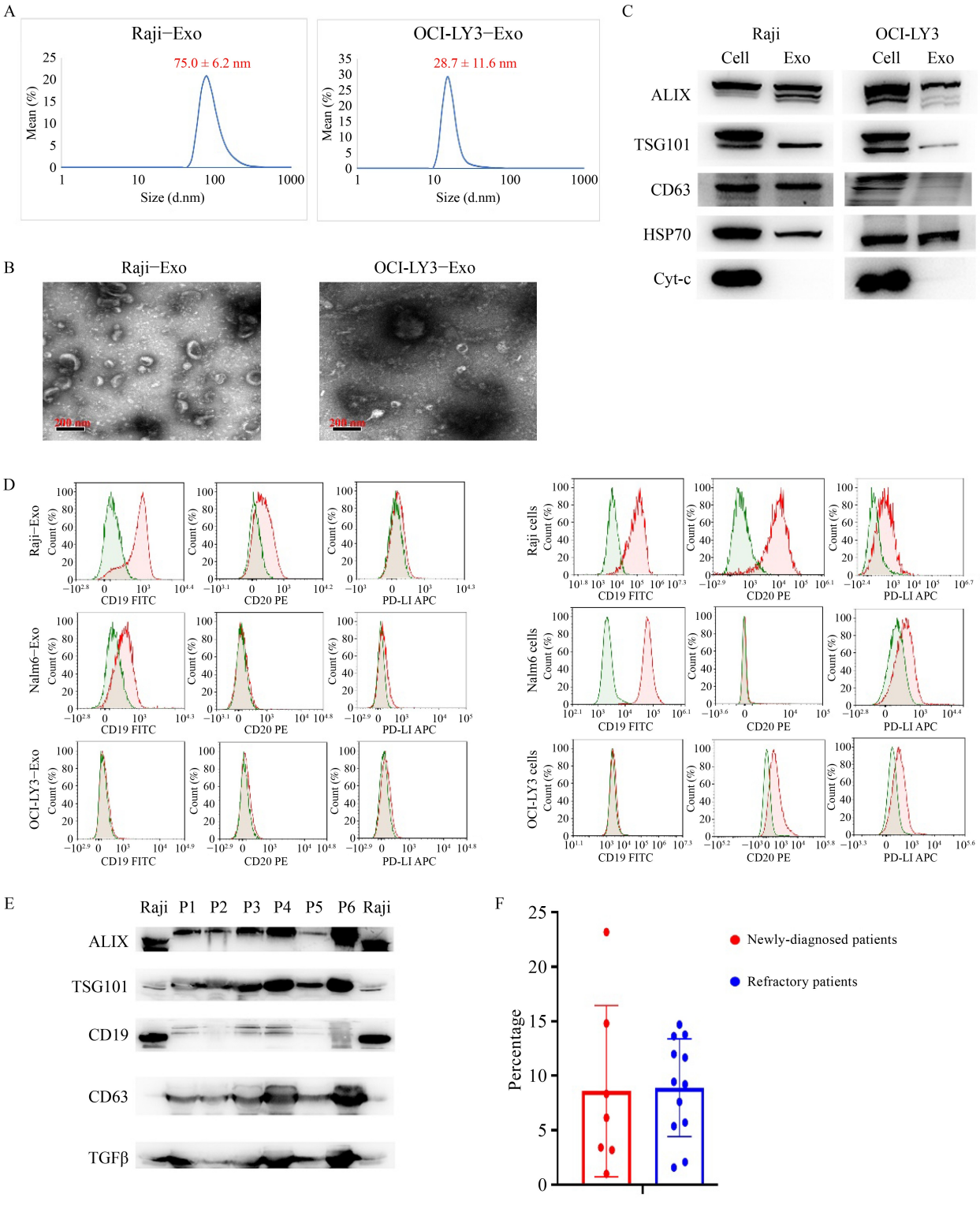

Fig. 1 Characterization and surface markers of exosomes from B-cell malignancies. (A) Size distribution of exosomes from lymphoma cell lines was determined by dynamic light scattering (DLS). (B) Transmission electron micrographs of the exosomes. Scale bars = 200 nm. (C) Western blot for exosome markers (ALIX, TSG101, and CD63) and cellular proteins in Raji–Exo or OCI-LY3–Exo. (D) Flow cytometry analysis of CD19, CD20, and PD-L1 expression on the surfaces of exosomes and their parental tumor cells. The green histograms represent the isotype-matched control mAbs for indicated fluorescent antibodies, whereas the red histograms indicate positive fluorescence. (E) Western blot for determining exosome markers (ALIX, TSG101, and CD63) and TGF-β in exosomes from six patients with B-cell lymphoma. (F) CD19 expression on the surface of exosomes from 18 patients with newly-diagnosed or refractory/relapsed B-cell lymphoma was analyzed through flow cytometry. Data are mean ± S.D.

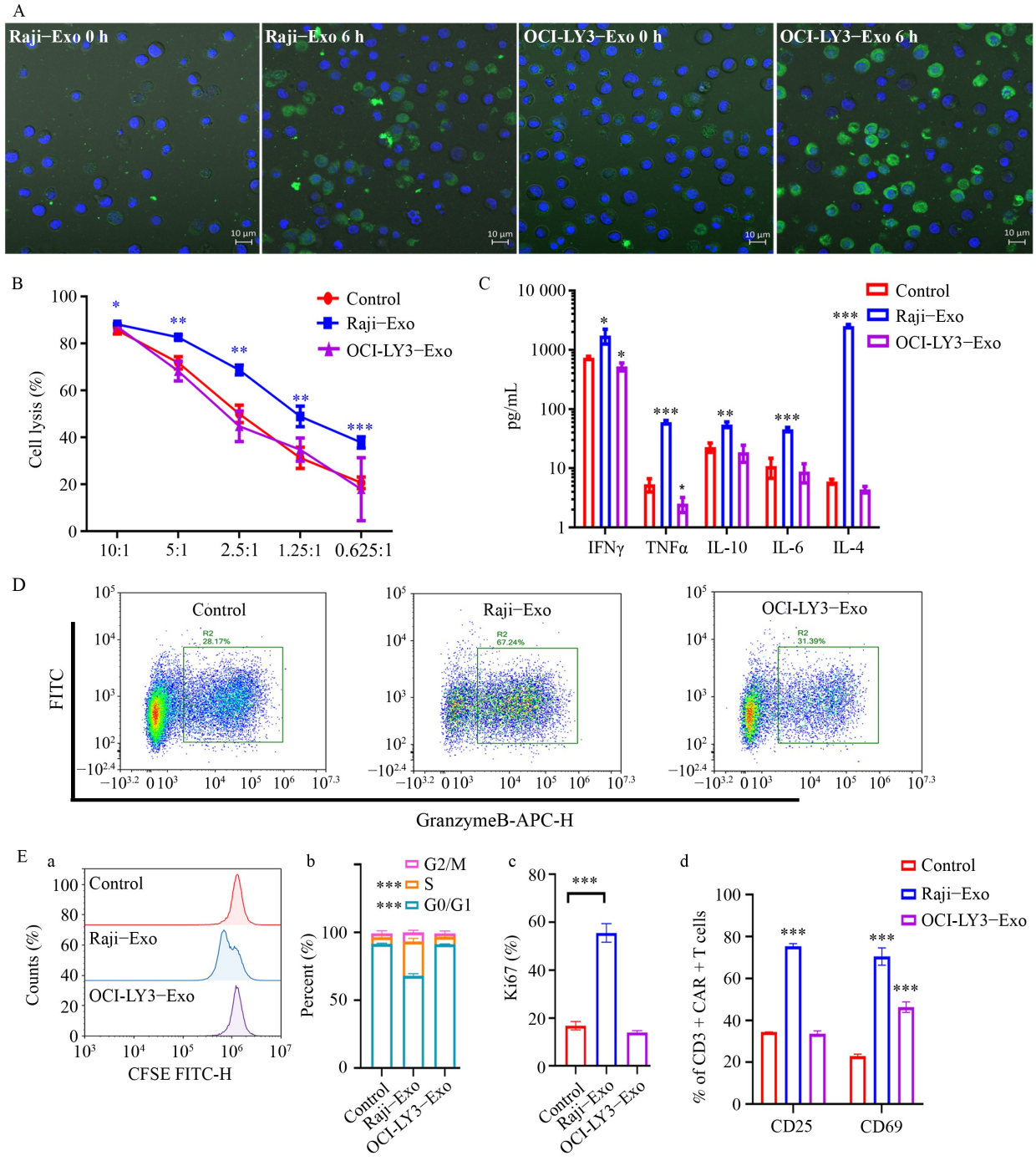

Fig. 2 Priming with CD19-contained lymphoma exosomes activates CD19-specific CAR T-cells. (A) CD19-specific CAR T-cells stained with Hoechst 33 258 (1 μg/mL) were cultured with PKH67-labeled exosomes (100 μg/mL) derived from Raji or OCI-LY3 cells, and the uptake of exosomes was photographed by confocal laser scanning microscopy at 0 and 6 h. Green represents PKH67-labeled exosomes; blue represents CAR T-cells' nuclei. (B) Killing activity of CAR T-cells that primed with 100 μg/mL Raji–Exo or OCI-LY3–Exo in response to tumor cells. The cytotoxic activity of CAR-T against tumor cells Raji–Luc–GFP was assessed by a luminescence-mediated cytotoxic assay at effector-to-target (E:T) ratios of 10:1, 5:1, 2.5:1, 1.25:1, and 0.625:1 for 4 h. (C) CAR T-cells were cocultured with or without exosomes (100 μg/mL) for 48 h. The concentration of IFN-γ, TNF-α, IL-10, IL-6, and IL-4 cytokines in the coculture system were measured by cytometric bead array (CBA) human Th1/Th2 cytokine kit. (D) Flow cytometry analyses the expression of granzyme B in Raji or OCI-LY3 exosome–pretreated CAR T-cells. (E) (a) CAR T-cells (1×10^5 cells) were stained with 1 μmol/L CFSE dye at 37 °C in the dark for 30 min and then treated with Raji or OCI-LY3-exosomes (100 μg/mL) for 48 h. The dilution of CFSE was evaluated through flow cytometry analysis in each group. Flow cytometry analyses the cell cycle (b) and expression of Ki-67 (c) and CD25 and CD69 (d) in the CAR T-cells, which were exposed to indicated exosomes for 48 h. Data are represented as mean ± S.D of three independent biological replicates. *P* values were obtained from unpaired two-tailed Student's *t*-tests. $*P < 0.05$, $**P < 0.01$, $***P < 0.001$.

Initial activation of CAR T-cells is dependent on exosomal CD19 antigen

The architecture of CAR molecule triggers a potent T-cell receptor–independent T-cell response upon antigen encounter [9]. We speculated that the activation of CAR T-cells by lymphoma TEXs was mainly due to the exosomal CD19 antigen. To confirm this hypothesis, we then established a Raij CD19$^{-/-}$ cell line, a derivative of Raji cell line with CD19 gene KO. The exosomes derived from Raij CD19$^{-/-}$ cells were negative for CD19 antigen expression (Fig. 3A). Next, we investigated the effect of

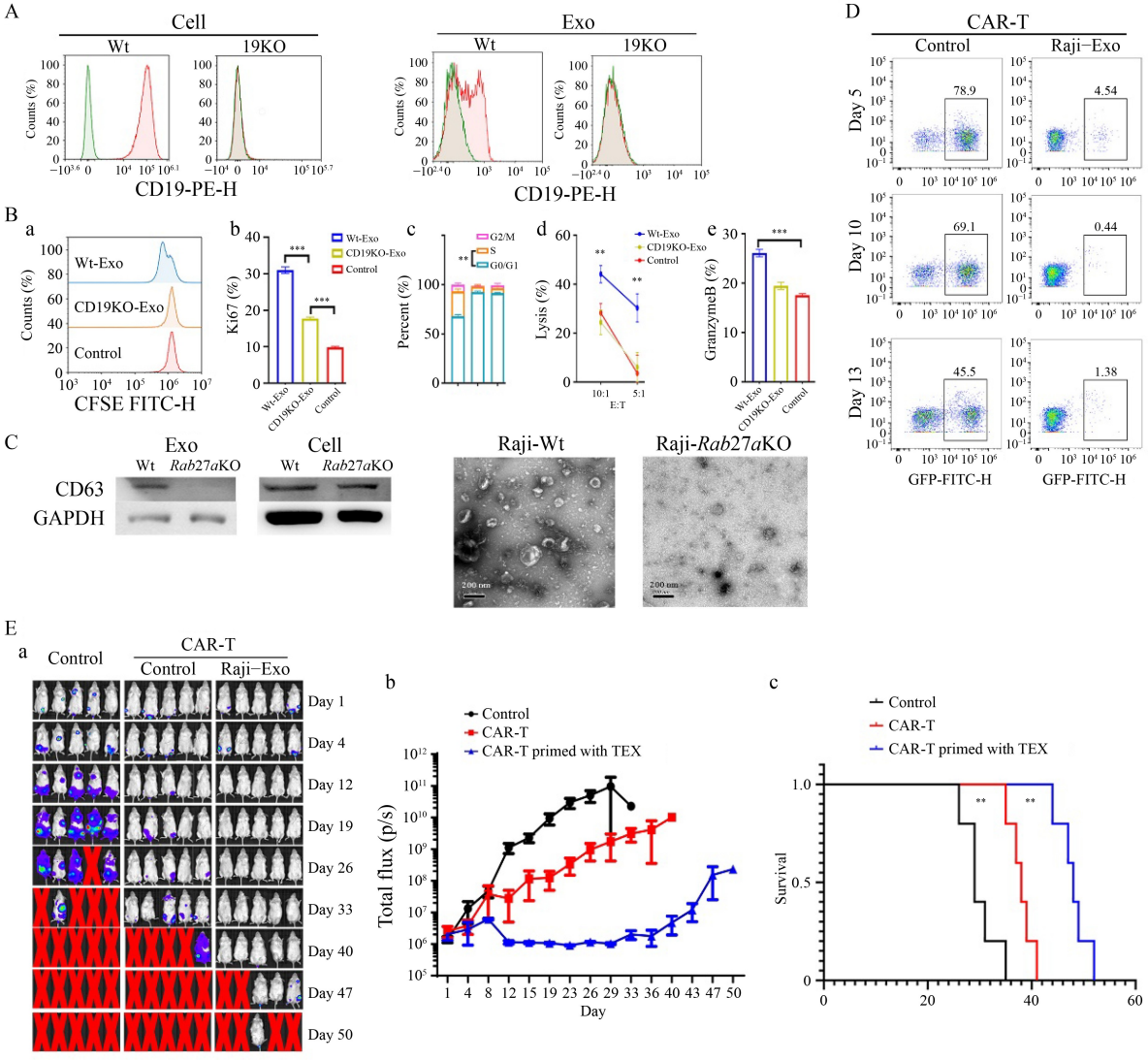

Fig. 3 Initial activation of CAR T-cells is dependent on exosomal CD19 antigen. (A) The expression of CD19 on the surface of wide-type (Wt) Raji, CD19-KO Raji cells, or their derived exosomes. Red histogram indicates PE-conjugated CD19 antibody fluorescence. The green histogram represents PE isotype Ctrl antibody fluorescence. (B) (a) CFSE-mediated proliferation of CAR-T cocultured with Wt Raji or CD19-KO Raji–Exo was analyzed. Spared CAR-T served as the control. CAR T-cells were exposed to Wt Raji or CD19-KO Raji–Exo for 48 h, and the expression of Ki-67 (b), cell cycle (c), cytotoxicity (d), and the secretion of granzyme B (e) were analyzed. (C) Western blot for exosome marker protein CD63 in Raji–Exo or Raji–*Rab27a* KO cells (left). Transmission electron micrographs of exosomes in Raji–Exo or Raji–*Rab27a*KO cells (right). Scale bars = 200 nm. (D) Long-term cytotoxicity of CAR T-cells exposed to Raji–Exo on Raji–*Rab27a* KO-GFP cells. CAR T-cells were pulsed with the Raji–Exo or not for 48 h and cocultured with Raji–*Rab27a* KO-GFP cells at an E:T ratio of 1:4 for 5, 10, and 13 days. Flow cytometry analyses the expression of residual GFP^{+} tumor cells at indicated times. (E) *In vivo* antitumor effect of Raji–Exo-pretreated CAR T-cells. NSG mice were injected intravenously with Raji–*Rab27a* KO-GFP-luciferase cells (1×10^5) on day −5 and treated with CD19–CAR-T or Raji–Exo-primed CD19–CAR T-cells (1×10^6) on day 0. PBS was injected into the control group. (a) The tumor burden was measured using bioluminescence imaging; (b) Total bioluminescence was traced in CAR-T, Raji–Exo-primed CAR T-cells, and control group; (c) Kaplan–Meier analysis of mice survival curve. Error bars represent SEM. *P* values were calculated using unpaired two-tailed Student's *t*-tests. $^{*}P < 0.05$, $^{**}P < 0.01$, $^{***}P < 0.001$.

Raij CD19$^{-/-}$ TEXs on CD19–CAR T-cells. As expected, we found that priming with Raij CD19$^{-/-}$ TEXs did not affect the proliferation and activation or the cytotoxicity of CAR T-cells (Fig. 3B). *Rab27a*, an important exosomal biogenesis gene, is essential for exosome secretion [22]. In the present study, *Rab27a* was knocked out in Raji cells by CRISPR/Cas9-mediated mutagenesis, which led to the loss of almost all exosomes (Fig. 3C). We evaluated cytotoxic activity of CAR T-cells primed with Raji TEXs against Raij Rab27a$^{-/-}$ cells. As shown in Fig. 3D, an enhanced cytolytic activity was observed in the Raij Rab27a$^{-/-}$ cells. To further confirm the enhanced CAR T-cell activation stimulated by exosomal CD19 antigen *in vivo*, we established two animal models bearing luciferase-expressing Raji cells or Raij Rab27a$^{-/-}$ cells. In the Raji animal model, Raji–Exo-primed CAR T-cells present antitumor activity similar to that of the unprimed CAR T-cells (Fig. S2), suggesting TEXs produced by wild-type Raji cells counteracted the initial activation of CAR T-cells. Whereas, in the mice bearing Raij Rab27a$^{-/-}$ model, Raji TEX-primed CAR T-cells exerted a stronger antitumor efficacy, thereby resulting in significantly improved survival compared with parent CAR T-cell treatment (Fig. 3E).

Prolonged presence of lymphoma TEXs impairs the effector functions of CAR T-cell

Persisting antigenic stimulation during cancer immunotherapy can result in T-cell exhaustion, a state of dysfunction, accompanied by the high expression levels of inhibitory receptors, such as PD-1, Tim3, and LAG3, and defective immune memory [22]. TEXs from solid tumors and chronic lymphocytic leukemia (CLL) cells promote the dysfunction and exhaustion of CAR T-cells [12,21]. Therefore, we investigated whether B-cell lymphoma exosomes can influence CAR T-cell function, mainly focusing on cell apoptosis and associated factors, such as the upregulated expression of immune checkpoint molecules and differentiated phenotypes of CAR T-cells. The CAR T-cells showed a dose-dependent decrease in cell viability measured by MTT assay after treatment with Raji TEXs for 6 h (Fig. 4A). When CAR T-cells were cultured with Raji TEXs for 48 h, we observed significantly greater death of CAR T-cells with significantly increased expression levels of immune checkpoint molecules PD-1, TIM3, and LAG3 than that in untreated counterparts (Fig. 4B). Whereas, the level of TIM3 rather than the levels of PD-1 and LAG3 was elevated on the CAR T-cells treated with OCI-LY3 TEXs (Fig. 4C). In addition, Raji TEX-primed CAR T-cells showed an increased proportion of differentiated phenotype (T_{EFF}) and low proportions of T_{CM} and naïve phenotype (Fig. 4D). Considering that CAR T-cell products used in clinics are usually generated from autologous T-cells, we evaluated the effects of TEXs on CAR T-cells derived from four patients. The patients' characteristics are listed in Table S1. All CAR T-cells from the patients exhibited a tendency to exhibit initial activation and final dysfunction mediated by priming with Raji TEXs (Fig. S3). We hypothesized that persistent TEX exposure eventually leads to inactive CAR T-cell function, which in turn induces immunotherapy resistance. To verify this hypothesis, CAR T-cells primed with Raji TEXs or unprimed CAR T-cells were cultured in the presence or absence of Raji TEXs for 6 h, and cytotoxicity was then evaluated. The results indicated reduced cytotoxicity in primed and unprimed CAR T-cells after prolonged exposure to Raji TEXs (Fig. 4E). We then examined whether plasma exosomes from patients altered the expression of the inhibitory receptors of CAR T-cells and terminal differentiation. Notably, our results demonstrated that the expression levels of PD-1 and LAG3 were upregulated after exposure to plasma exosomes from two patients (Fig. 4F). We found increased frequency of T_{EFF} and reduced frequency of $T_{Naïve}$ cells upon coculture with plasma exosomes (Fig. 4G). Then, we studied the impact of patients' exosomes on the conversion of the Tregs of CAR T-cells. Increased frequencies of Tregs were observed in all the CAR T-cells from three cases, which were cocultured with the exosomes of patient 2. Such a tendency was observed in the CAR T-cells from only one case when cocultured with the exosomes of patient 1 (Fig. 4H).

Single-cell transcriptome profiling of CAR T-cells after Raji TEX exposure

To better understand the molecular changes of CAR T after Raji TEX exposure, we performed scRNA-seq on 46 809 single CAR T-cells from three patients. The patients' characteristics are listed in Table S1. Using dimensionality reduction with the UMAP method, we visualized and identified 14 clusters (Fig. 5A). Heatmap shows top 10 differentially expressed genes of each identified cluster (Fig. 5B). Then we compared clusters between CAR T and CAR T-cells primed with Raji TEXs, and found a significantly increased abundance of CD4–LTA cluster and decreased abundance of CD4–SESN3 cluster within CAR T-cells primed with Raji TEXs (Fig. 5C). The results of GSEA analysis showed that genes in effector and activated T-cells were significantly enriched in CD4–LTA. Whereas, CD4–SESN3 cluster showed the significant enrichment of genes involved in $T_{Naïve}$ and unstimulated T-cells (Fig. 5D).

We analyzed the differentially expressed genes, which are related to the T-cell function and phenotype, between TEX-priming CAR and untreated CAR T-cells. Upregulated genes in TEX-primed CAR T-cells were involved in pathways of cell proliferation, activation,

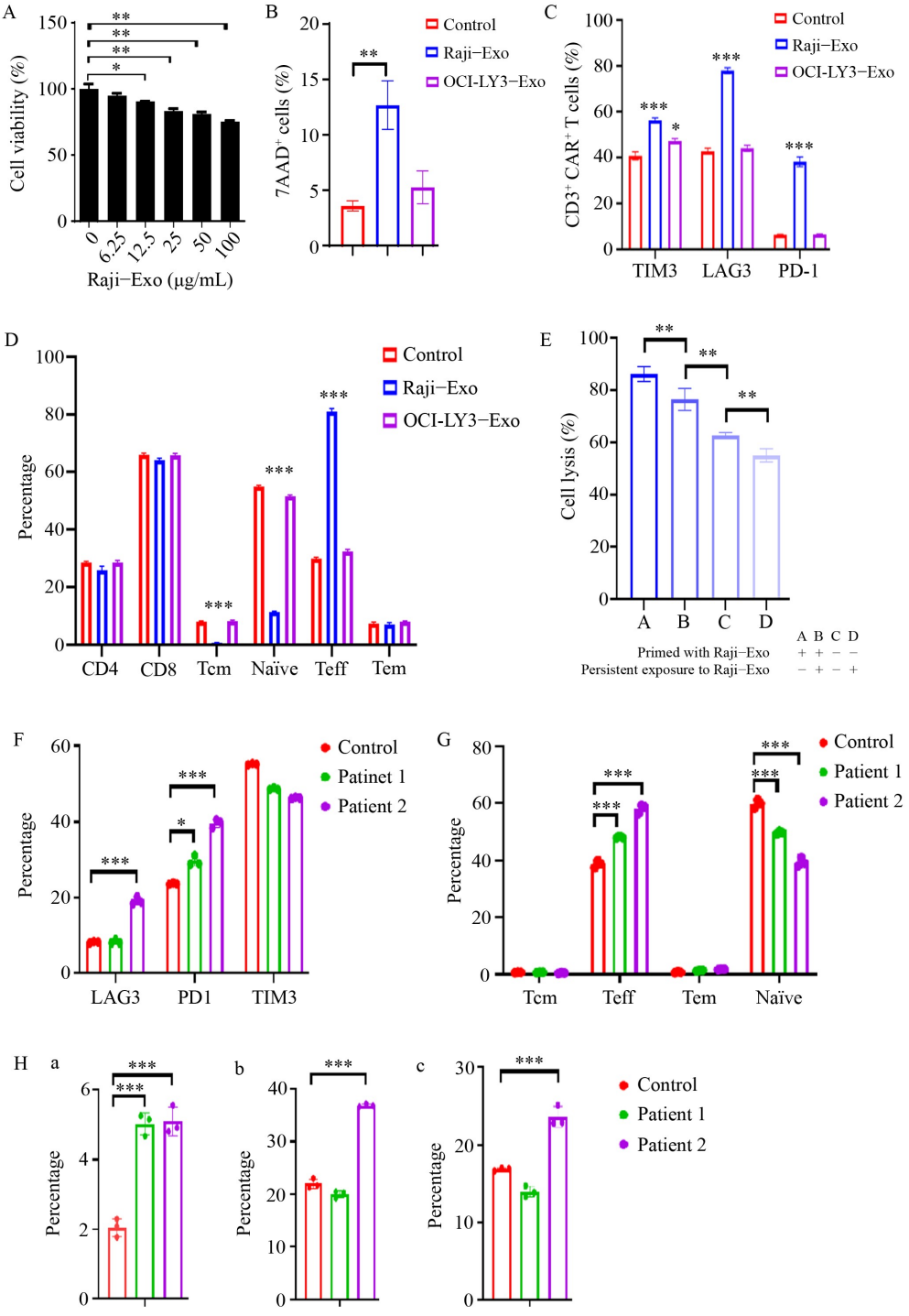

Fig. 4 TEXs and plasma exosomes from patients with lymphoma impair the effector functions of CAR T-cells. (A) CAR T-cells were exposed to a dose escalation of the Raji–Exo for 6 h, and cell viability was determined using MTT assay. The expression of 7AAD. (B) TIM-3, LAG-3, and PD-1. (C) and the differentiation of T_{CM} ($CD45RA^{-}CD62L^{+}$), $T_{Naïve}$ ($CD45RA^{+}CD62L^{+}$), T_{EFF} ($CD45RA^{+}CD62L^{-}$), and T_{EM} ($CD45RA^{-}CD62L^{-}$). (D) Analysis by flow cytometry after CAR T-cells were exposed to Raji–Exo for 48 h. (E) CAR T-cells primed with or without Raji–Exo were cocultured in the presence or absence of Raji TEXs with Raji–Luc–GFP cells for 6 h, and a luminescence-mediated cytotoxic assay was performed for cytotoxicity evaluation. CAR T-cells were exposed to plasma exosomes (100 μg/mL) from two patients for 48 h, the expression of TIM-3, LAG-3, and PD-1 (F), and the differentiation of T_{CM} ($CD45RA^{-}CD62L^{+}$), $T_{Naïve}$ ($CD45RA^{+}CD62L^{+}$), T_{EFF} ($CD45RA^{+}CD62L^{-}$), and T_{EM} ($CD45RA^{-}CD62L^{-}$) (G) were analyzed by flow cytometry. (H) CAR T-cells derived from three different patients were cocultured with plasma exosomes (100 μg/mL) from two patients for 48 h and then analyzed through flow cytometry to determine the percent of Tregs ($CD4^{+}CD25^{+}FOXP3^{+}$). *P* values were obtained through unpaired two-tailed Student's *t*-tests. $^{*}P < 0.05$, $^{**}P < 0.01$, $^{***}P < 0.001$.

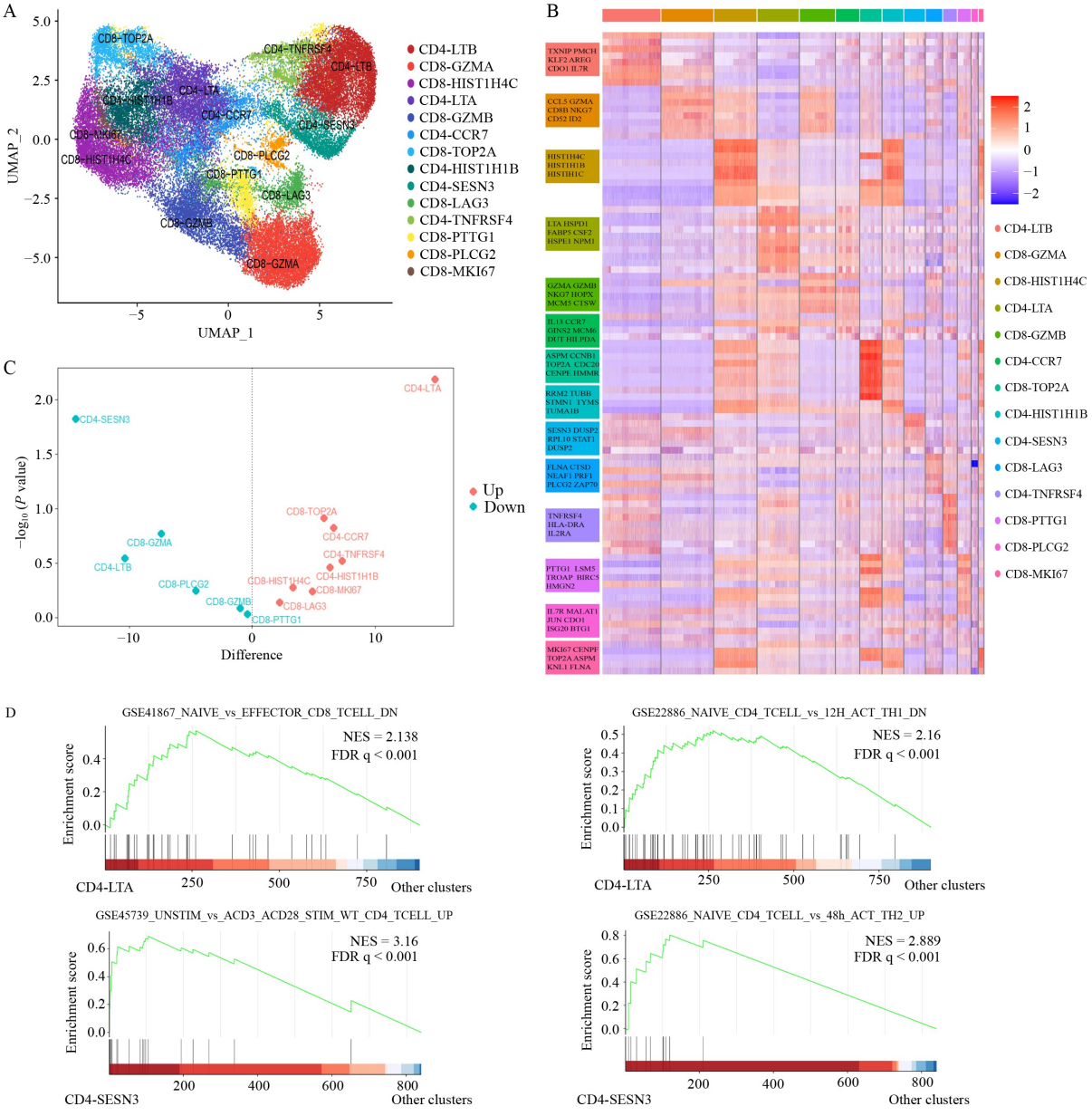

Fig. 5 Single-cell transcriptional profiling of CAR T-cells after Raji TEX exposure. (A) The UMAP plot shows the annotation and color codes for cell types of the CAR T-cells derived from three different patients. (B) Heatmap showing the expression of marker genes in the indicated cell types. The top genes are shown on the left. (C) Plot depicts the differences in the proportion of clusters between the CAR T primed with Raji–Exo and untreated CAR T-cells. Red dots indicate that the proportions of these clusters increased in CAR T-cells primed with the Raji–Exo group, and the blue dots mean a decrease. (D) The graphs show the results of a GSEA performed for the indicated gene sets in Raji–Exo-exposed CAR T-cells. The normalized enrichment Score (NES) and false discovery rate (FDR) are indicated.

cytotoxicity, chemotaxis, transfactors, and exhaustion. Notably, naïve/memory cell markers, such as IL-7R, LEF1, SELL, and JUNB, were downregulated in TEX-primed CAR T-cells (Fig. 6A). Pseudo-time analysis indicated that the less differentiated phenotypes were at the beginning of the trajectory path, whereas the more differentiated phenotypes were at a terminal state (Fig. 6B). After treatment with TEX, the expression of genes related to cellular proliferation and cytotoxicity, such as CD69 and GZMB, increased. However, dynamic cell transition analysis showed the upregulated expression of terminally exhausted T-cell marker genes, including *LAG3* and *TIM3* (HAVCR2; Fig. 6C).

Exosomal TGF-β contributes to the conversion of CAR T-cells into Tregs and terminal differentiated phenotype

In UMAP analysis, CAR T-cells were grouped mainly according to T-cell subtypes as annotated based on a

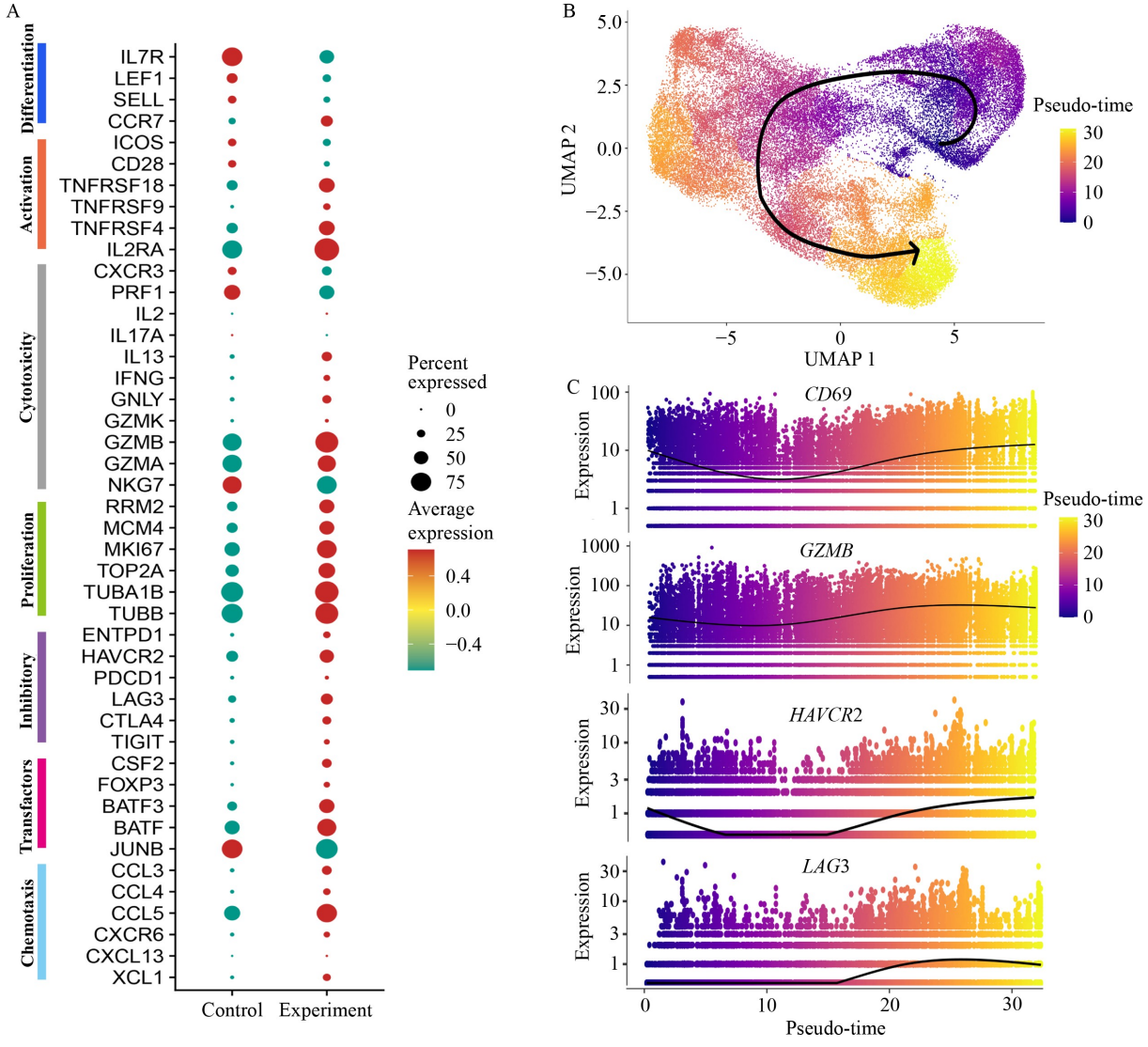

Fig. 6 Analysis of differentially expressed gene related to the T-cell function and phenotype of CAR T-cells after Raji–Exo exposure by single-cell transcriptional profiling. (A) Dot plot illustrates the expression level of genes associated with differentiation, activation, cytotoxicity, proliferation, immune inhibitory, transactions, and chemotaxis in Raji–Exo-exposed CAR T-cell (experiment) and untreated CAR T-cells (control). The size of the circle represents the percentage of cells expressing the gene in each cluster, and the color depicts how highly expressed the gene is within that cluster. (B) Monocle3 trajectory analysis of CAR T-cells. The color represents the stage of cell growth. The black arrow shows the pseudo-time trajectory of the cell growth. (C) The expression of genes (*CD69*, *GZMB*, *HAVCR2*, and *LAG3*) during the pseudo-time trajectory.

panels of known cell lineage–specific genes. We found that the number of $Foxp3^+$ cells significantly increased in the presence of TEXs (Fig. 7A). Subsequently, increase in $CD4^+$ $CD25^+$ $Foxp3^+$ cells within CAR T-cells primed with TEXs was confirmed by flow cytometry analysis, and the overexpression of Foxp3 gene was demonstrated by real-time PCR (Fig. 7B). TGF-β produced by tumor cells play a key role in immune escape via the conversion and expansion of Tregs and induce T-cell exhaustion [28–30]. We then explored whether lymphoma exosomal TGF-β can result in the expansion of Tregs and exhaustion of CAR T-cells. As validated by Western blot analysis, Raji and OCI-LY3 TEXs contained TGF-β (Fig. 7C). Previous studies have shown that Smad3 is required for the TGF-β-mediated conversion of $CD4^+$ $CD25^-$ T-cells to $CD4^+$ $CD25^{hi}$ $FOXP3^+$ Tregs [31,32]. We observed that phosphorylated Smad3 was upregulated in the CAR T-cells primed with Raji TEXs and that LY2109761 (a TGF-β inhibitor) significantly inhibited the activation of Smad3 (Fig. 7D). Having verified that exosomal TGF-β activates Smad3 in CAR T-cells, we next investigated whether TGF-β inhibition by LY2109761 could reverse conversion and differentiation of CAR T-cells mediated through TEXs exposure. To this end, TEX-primed CAR T-cells were cocultured with or without LY2109761 at different doses, and the cells from

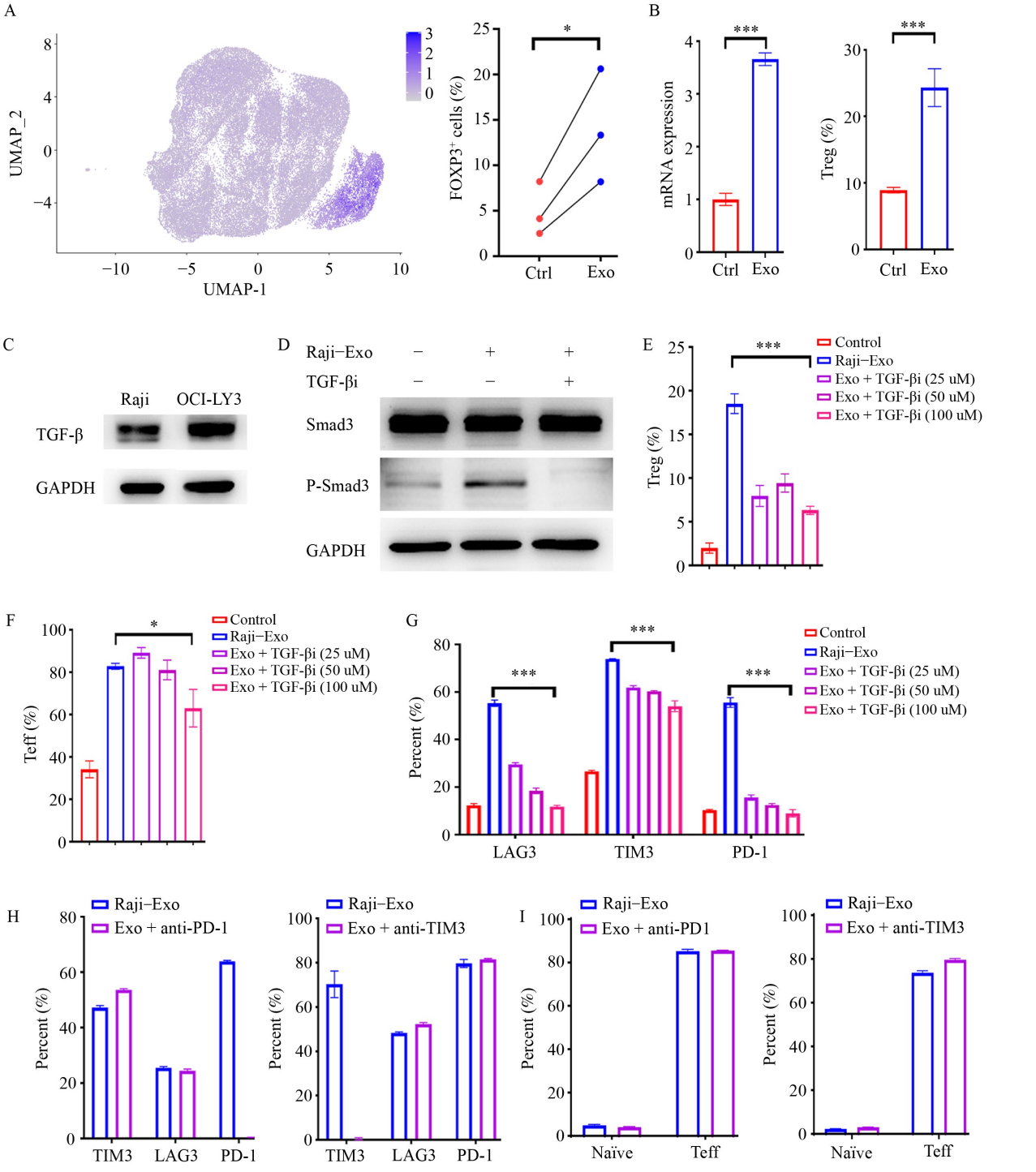

Fig. 7 Exosomal transforming growth factor β contributes to the conversion of CAR T-cells into Tregs and terminal differentiated phenotype. (A) UMAP plot shows the expression pattern of FOXP3. Color intensity represents expression level (left). The percentage of $FOXP3^+$ cells was shown in the experimental and control groups (Right). (B) Real-time PCR (left) and flow cytometry (right) were performed for the analysis of FOXP3 expression after CAR T-cells were primed with Raji–Exo for 48 h. (C) Expression of TGF-β in Raji–Exo and OCI-LY3–Exo by Western blots analysis. (D) Western blot was performed for the analysis of SMAD3 and p-SMAD3 expression in CAR T-cells cocultured with Raji–Exo in the presence or absence of the TGF-β inhibitor LY2109761 (100 μmol/L). CAR T-cells alone or CAR T-cells cocultured with Raji–Exo in the presence of 0, 25, 50, and 100 μmol/L LY2109761 for 48 h, and then flow cytometry analyses were performed to determine the percentages of Tregs ($CD4^+CD25^+FOXP3^+$) (E), T_{EFF} ($CD62L^-CD45RA^+$) (F), and the expression of LAG-3, TIM-3, and PD-1 (G). CAR T-cells were cocultured with Raji–Exo and PD-1 inhibitor (IBI308, 30 μg/mL) or LAG3 inhibitor (SHR-1702, 40 μg/mL) for 48 h, and the expression levels of LAG3, TIM3, and PD-1 on the surfaces of CAR T-cells (H) and differentiated phenotypes (I) were analyzed by flow cytometry. *P* values were from unpaired two-tailed Student's *t*-tests. $*P < 0.05$, $**P < 0.01$, $***P < 0.001$.

different conditions were analyzed for Treg expansion and effector and $T_{Naïve}$ cell differentiation using flow cytometry. Interestingly, in the presence of LY2109761, TEX-induced Treg expansion and terminal differentiation were partially reversed (Fig. 7E and 7F). On the other hand, we also found that LY2109761 significantly decreased TEX-induced upregulated expression of immune checkpoints, including PD-1, Tim3, and LAG3, in a dose-dependent manner (Fig. 7G), supporting the important roles for TGF-β in upregulation of PD-1, which was *Smad3*-dependent in antigen-specific T-cells [33]. Although the inhibition of PD1 or TIM3 by relevant mAb were confirmed (Fig. 7H), neither anti-PD-1 nor anti-TIM3 mAbs was able to rescue the TEX-mediated phenotype (Fig. 7I). These findings suggested that exosomal TGF-β is mainly responsible for the impaired function of CAR T-cells.

CD19–CAR T-cells combined with TGF-β inhibitor eliminate B-cell lymphoma

Finally, to confirm the *in vivo* enhanced antitumor effects of combinatorial treatment regimen of CD19-specific CAR T-cell and TGF-β inhibitor LY2109761, we performed a lymphoma cell xenograft model established through vein injection of 1×10^5 of Raji–Luc cells into NSG mice. After engraftment of Raji cells for five days, LY2109761 was administered to the mice to receive a combination treatment. After 2 days, the mice were treated with vehicle, CAR T-cells (1×10^6 cells), or CAR T-cells combined with LY2109761, respectively. In the combinatorial groups, LY2109761 (50 mg or 100 mg/kg bodyweight, Bid, for 5 days per week for up to 8 weeks) was given to tumor-bearing mice by oral administration (Fig. 8A). We showed that either CD19–CAR T-cells or CAR T-cells combined with 50 mg/kg LY2109761 was able to significantly inhibit tumor progression, which resulted in the loss of luminescence signals in 1/5 of the animals. Notably, a combination of CAR T-cells and high-dose LY2109761 (100 mg/kg) dramatically inhibited tumor development, and the effect was accompanied by the loss of luminescence signals in 5/5 of the mice (Fig. 8B). In addition, the effect significantly prolonged survival (Fig. 8C). These data suggest a strong synergism between the two therapeutic agents.

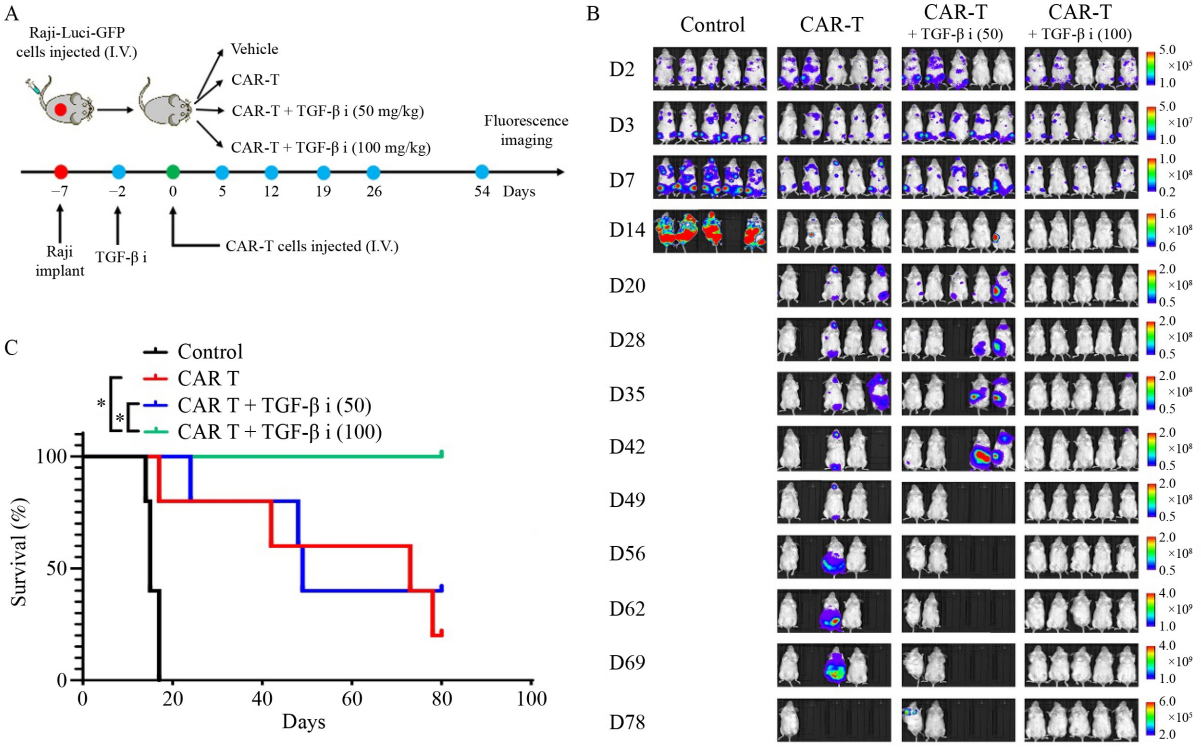

Fig. 8 CD19–CAR T-cells combined with TGF-β inhibitor eliminate B-cell lymphoma. (A) Schematic of experimental design. Briefly, mice were transplanted with Raji–Luc–EGFP cells (1×10^5) on day 7. Mice began to receive combination treatment of TGF-β inhibitor (LY2109761, 50 mg or 100 mg/kg twice daily by oral) on Day −2. On Day 0, mice were treated with PBS, CAR T-cells (1×10^6 cells) or CAR T-cells combined with LY2109761. In the combinatorial groups, LY2109761 (50 or 100 mg/kg twice daily orally, 5 days per week for 8 weeks) was administrated. (B) The tumor burden was measured using bioluminescence imaging. Total bioluminescence was traced in the vehicle, CAR T-cells combined with the LY2109761 group, and CAR T-cells. Error bars represent SEM. (C) Kaplan–Meier analysis of mice survival curve. *P* values were calculated using unpaired two-tailed Student's *t*-tests. $*P < 0.05$.

Discussion

Tumor-derived exosomes have been implicated in cell–cell communication and the transfer of oncogenic and immunosuppressive molecules between cancer cells and cells in the microenvironment, thereby promoting cancer progression and suppressing immune responses [17–19]. TEX can impair the function and proliferation of T-cells and induce the exhausted phenotype of T-cells through the delivery of surface ligands, proteins, and miRNA content [16,21]. However, the relationship between TEXs and CAR T-cells remains largely unclear. CARs are genetically engineered synthetic receptors that function to recognize and kill tumor cells through binding to target antigens, and their effect is independent from antigen presentation process enforced by the MHC receptor. The importance of exosomal B-cell antigens has been demonstrated, and CD20-expressing lymphoma exosomes can bind to therapeutic anti-CD20 antibody rituximab, which in turn reduces available antibodies that would bind to tumor cells, eventually protecting target cells from antibody attack [25,34]. In this study, we demonstrated that CD19-specific CAR T-cells shortly pre-exposed to lymphoma cell-derived TEXs exhibited enhanced proliferative and cytotoxic capacities and that the TEX-induced activation of CAR T-cells requires the presence of exosomal CD19 in the TEX cargo. We also demonstrated that CD19–CAR T-cells subjected to short-term priming with Raji TEXs are therapeutically superior to unprimed CAR T-cells in a mouse model of Raij Rab27a$^{-/-}$ cells that did not produce exosomes. These data suggest that lymphoma cell-derived exosomal CD19 binds to the antigen binding domain of CD19–CAR and then activates CAR T-cells.

TEXs impede T-cell antitumor immune responses via their immunosuppressive cargo [16,18], but the relationship between TEXs and the functions of CAR T-cells have not been comprehensively explored [26,35]. Recently, Ali and colleagues [36] reported that neuroblastoma-derived exosomes inhibited the function of CD171-sepecific CD4$^+$, but not CD8$^+$ CAR T-cells, suggesting CD4$^+$ T-cells are sensitive toward TEXs. Although lymphoma derived TEXs exhibited capacity of initial activation of CAR T-cells, it also may induce CAR T-cell apoptosis and impair tumor cytotoxicity of CD19-specific CAR T-cells under longer exposure. Notably, longer coculture of CAR T-cells with Raji TEXs led to more profound inhibition of cytolytic capacity. We also found that lymphoma TEXs upregulated the expression of inhibitory receptors PD-1, TIM3, and LAG3, which may lead to apoptosis of T-cells and subsequently result in tumor immune escape [20]. Moreover, CAR T-cells displayed a terminally differentiated phenotype after exposure to the TEXs. These findings are consistent with a recent report regarding the effect of TEXs on CAR T-cells, raising a caveat that CLL-derived exosomes induce a state of CD19-specific CAR T dysfunction characterized by impaired antitumor activity, increased expression of CTLA-4 and TIM3, and upregulated gene expression of AP-1 (FOS–JUN) and YY1 pathway, which represent T-cell exhaustion [26]. Although we observed significant increase of PD-1, TIM3, and LAG3 expression in CAR T-cells treated with lymphoma TEX, similar to a previous report [26], we failed to reverse the impaired CAR T function after PD-1 or TIM3 blockade alone. These findings indicate that there may be an intrinsic mechanism of lymphoma TEXs, rather than immune inhibitory receptors/ligands interactions, responsible for this CAR T-cell dysfunction.

Increasing evidence suggests that CAR T-cells possessing a less differentiated phenotype such as T_{CM} and T_{SCM} cells are associated with superior antitumor activity [37]. The expansion and persistence of CAR T-cells and a central memory phenotype are correlated with improved clinical response [38,39]. On the basis of our findings, we performed scRNA-seq to identify differences in the transcriptional, phenotypic, and functional profiles of CAR T-cells at basal levels or after treatment with TEX. The results showed the TEX-mediated initial activation of CAR T-cells as evidenced by their increased expression of CD69 and GZMB. However, we found that, at basal condition, CAR T-cells had conserved differentiation status, including naïve and memory phenotypes, whereas TEX-treated CAR T-cells exhibited more differentiated phenotypes. More importantly, we observed the increased expression level of FOXP3 in CD4$^+$ CAR T-cells treated with Raji TEXs. This finding strongly suggests that lymphoma TEXs can directly convert CAR T-cells into Tregs and was further verified by flow cytometry analysis. TGF-β, one of the most important regulators in the TME, is enriched in exosomes released by a wide range of tumors and play a key role in Treg conversion and expansion [28–30,40]. Here, we showed that TGF-β is enriched in Raji TEXs. By blocking TGF-β/Smad3 signaling with LY2109761, we were able to rescue the negative effects of TEXs on Treg conversion, terminal differentiation, and expression of immune checkpoint in the CAR T-cells. Blocking TGF-β signaling by multiple routes, such as gene editing, TGF-β antibody, TGF-β dominant-negative receptor II, TGF-β/IL-7 chimeric switch receptor, TGF-β trap protein, and TGF-β-receptor kinase inhibitor, is a promising strategy for reversing TGF-β-driven immune suppression and enhancing tumor elimination by CAR T-cells [23,30,41–43]. In the subsequent *in vivo* study with a mouse model of Raji cell xenografts, we demonstrated that the TGF-β inhibitor LY2109761 allows for enhanced antitumor responses when using CD19-specific CAR T-cells, resulting in tumor eradication and yielding long-

term survival benefits to mice. We selected the TGF-β inhibitor in this study because the treatment of refractory, advanced, and metastatic malignancies using TGF-β inhibitors, such as AVID200, has been already ongoing in clinical trial phases (ClinicalTrials.gov: NCT03834662). Overall, these results highlight that inhibiting the TGF-β pathway specific to a particular lymphoma-derived TEX can significantly improve CAR T-cell function in treating lymphoma and suggest a novel strategy of combining CAR T-cells with TGF-β inhibitor for overcoming acquired resistance to CAR T-cell treatment.

CLL-derived exosomes from patient plasma are potent systemic factors that directly induce exhaustion in CAR T-cells and impair antitumor activity [26]. Our data show that plasma exosomes from some patients with lymphoma induced the upregulation of inhibitory receptors, including PD-1 and LAG3, and the conversion of Tregs. These inconsistencies are likely to be associated with the heterogeneity in TGF-β expression across plasma exosomes from different patients. Compared with Raji TEX, plasma exosomes from patients contained lower levels of CD19. We speculated that another reason for these inconsistencies is that exosome isolation from the plasma of patients with lymphoma is more complex. Given that normal and lymphoma cells can produce corresponding exosomes, the isolated plasma exosomes were mixtures of exosomes in which TEXs might represent only a small part [44]. Thus, the pathophysiological link remains elusive.

In conclusion, our findings demonstrated adverse effect of lymphoma cell-derived exosomes on the functions of CD19–CAR T-cells, although the initial activation of CAR T-cells, which was dependent on exosomal CD19 molecule stimulation, was observed. Moreover, exosomal TGF-β might contribute to CAR T-cell apoptosis, upregulation of immune checkpoints, terminally differentiated phenotype, and conversion of Tregs induced by lymphoma TEXs, subsequently impairing the antigen-specific functions of CAR T-cells. Our results support that combinatorial treatment regimen of CAR T-cell therapy and TGF-β inhibitor can be clinically applied as a novel treatment strategy for refractory and relapsed B-cell lymphoma.

Acknowledgements

This work was supported by the funds from the National Natural Science Foundation of China (Nos. 81830006, 82170219, and 81830004), and the Science Technology Department of Zhejiang Province (No. 2021C03117).

Compliance with ethics guidelines

Conflicts of interests Yuanyuan Hao, Panpan Chen, Shanshan Guo, Mengyuan Li, Xueli Jin, Minghuan Zhang, Wenhai Deng, Ping Li, Wen Lei, Aibin Liang, and Wenbin Qian declare that they have no competing interests.

The study was approved by the responsible committee on human experimentation (institutional and national) and the study was performed in accordance with the ethical standards as laid down in the 1964 *Declaration of Helsinki* and its later amendments or comparable ethical standards. Informed consent was obtained from all patients for being included in the study. All institutional and national guidelines for the care and use of laboratory animals were followed.

Electronic Supplementary Material Supplementary material is available in the online version of this article at https://doi.org/10.1007/s11684-023-1010-1 and is accessible for authorized users.

References

1. Chong EA, Ruella M, Schuster SJ; Lymphoma Program Investigators at the University of Pennsylvania. Five-year outcomes for refractory b-cell lymphomas with car t-cell therapy. N Engl J Med 2021; 384(7): 673–674
2. Kochenderfer JN, Dudley ME, Kassim SH, Somerville RP, Carpenter RO, Stetler-Stevenson M, Yang JC, Phan GQ, Hughes MS, Sherry RM, Raffeld M, Feldman S, Lu L, Li YF, Ngo LT, Goy A, Feldman T, Spaner DE, Wang ML, Chen CC, Kranick SM, Nath A, Nathan DA, Morton KE, Toomey MA, Rosenberg SA. Chemotherapy-refractory diffuse large B-cell lymphoma and indolent B-cell malignancies can be effectively treated with autologous T cells expressing an anti-CD19 chimeric antigen receptor. J Clin Oncol 2015; 33(6): 540–549
3. Orlando EJ, Han X, Tribouley C, Wood PA, Leary RJ, Riester M, Levine JE, Qayed M, Grupp SA, Boyer M, De Moerloose B, Nemecek ER, Bittencourt H, Hiramatsu H, Buechner J, Davies SM, Verneris MR, Nguyen K, Brogdon JL, Bitter H, Morrissey M, Pierog P, Pantano S, Engelman JA, Winckler W. Genetic mechanisms of target antigen loss in CAR19 therapy of acute lymphoblastic leukemia. Nat Med 2018; 24(10): 1504–1506
4. Sotillo E, Barrett DM, Black KL, Bagashev A, Oldridge D, Wu G, Sussman R, Lanauze C, Ruella M, Gazzara MR, Martinez NM, Harrington CT, Chung EY, Perazzelli J, Hofmann TJ, Maude SL, Raman P, Barrera A, Gill S, Lacey SF, Melenhorst JJ, Allman D, Jacoby E, Fry T, Mackall C, Barash Y, Lynch KW, Maris JM, Grupp SA, Thomas-Tikhonenko A. Convergence of acquired mutations and alternative splicing of cd19 enables resistance to cart-19 immunotherapy. Cancer Discov 2015; 5(12): 1282–1295
5. Tong C, Zhang Y, Liu Y, Ji X, Zhang W, Guo Y, Han X, Ti D, Dai H, Wang C, Yang Q, Liu W, Wang Y, Wu Z, Han W. Optimized tandem CD19/CD20 CAR-engineered T cells in refractory/relapsed B-cell lymphoma. Blood 2020; 136(14): 1632–1644
6. Deng W, Chen P, Lei W, Xu Y, Xu N, Pu JJ, Liang A, Qian W. CD70-targeting CAR-T cells have potential activity against CD19-negative B-cell Lymphoma. Cancer Commun (Lond) 2021; 41(9): 925–929
7. Spiegel JY, Patel S, Muffly L, Hossain NM, Oak J, Baird JH, Frank MJ, Shiraz P, Sahaf B, Craig J, Iglesias M, Younes S, Natkunam Y, Ozawa MG, Yang E, Tamaresis J, Chinnasamy H,

Ehlinger Z, Reynolds W, Lynn R, Rotiroti MC, Gkitsas N, Arai S, Johnston L, Lowsky R, Majzner RG, Meyer E, Negrin RS, Rezvani AR, Sidana S, Shizuru J, Weng WK, Mullins C, Jacob A, Kirsch I, Bazzano M, Zhou J, Mackay S, Bornheimer SJ, Schultz L, Ramakrishna S, Davis KL, Kong KA, Shah NN, Qin H, Fry T, Feldman S, Mackall CL, Miklos DB. CAR T cells with dual targeting of CD19 and CD22 in adult patients with recurrent or refractory B cell malignancies: a phase 1 trial. Nat Med 2021; 27(8): 1419–1431

8. Cordoba S, Onuoha S, Thomas S, Pignataro DS, Hough R, Ghorashian S, Vora A, Bonney D, Veys P, Rao K, Lucchini G, Chiesa R, Chu J, Clark L, Fung MM, Smith K, Peticone C, Al-Hajj M, Baldan V, Ferrari M, Srivastava S, Jha R, Arce Vargas F, Duffy K, Day W, Virgo P, Wheeler L, Hancock J, Farzaneh F, Domning S, Zhang Y, Khokhar NZ, Peddareddigari VGR, Wynn R, Pule M, Amrolia PJ. CAR T cells with dual targeting of CD19 and CD22 in pediatric and young adult patients with relapsed or refractory B cell acute lymphoblastic leukemia: a phase 1 trial. Nat Med 2021; 27(10): 1797–1805
9. Liu H, Lei W, Zhang C, Yang C, Wei J, Guo Q, Guo X, Chen Z, Lu Y, Young KH, Lu Z, Qian W. CD19-specific CAR T cells that express a PD-1/CD28 chimeric switch-receptor are effective in patients with PD-L1-positive B-cell lymphoma. Clin Cancer Res 2021; 27(2): 473–484
10. Yan X, Chen D, Wang Y, Guo Y, Tong C, Wei J, Zhang Y, Wu Z, Han W. Identification of NOXA as a pivotal regulator of resistance to CAR T-cell therapy in B-cell malignancies. Signal Transduct Target Ther 2022; 7(1): 98
11. Milane L, Singh A, Mattheolabakis G, Suresh M, Amiji MM. Exosome mediated communication within the tumor microenvironment. J Control Release 2015; 219: 278–294
12. Mashouri L, Yousefi H, Aref AR, Ahadi AM, Molaei F, Alahari SK. Exosomes: composition, biogenesis, and mechanisms in cancer metastasis and drug resistance. Mol Cancer 2019; 18(1): 75
13. Whiteside TL. Tumor-derived exosomes and their role in cancer progression. Adv Clin Chem 2016; 74: 103–141
14. Yang E, Wang X, Gong Z, Yu M, Wu H, Zhang D. Exosome-mediated metabolic reprogramming: the emerging role in tumor microenvironment remodeling and its influence on cancer progression. Signal Transduct Target Ther 2020; 5(1): 242
15. Ghosh AK, Secreto CR, Knox TR, Ding W, Mukhopadhyay D, Kay NE. Circulating microvesicles in B-cell chronic lymphocytic leukemia can stimulate marrow stromal cells: implications for disease progression. Blood 2010; 115(9): 1755–1764
16. Ma F, Vayalil J, Lee G, Wang Y, Peng G. Emerging role of tumor-derived extracellular vesicles in T cell suppression and dysfunction in the tumor microenvironment. J Immunother Cancer 2021; 9(10): e003217
17. Szczepanski MJ, Szajnik M, Welsh A, Whiteside TL, Boyiadzis M. Blast-derived microvesicles in sera from patients with acute myeloid leukemia suppress natural killer cell function via membrane-associated transforming growth factor-beta1. Haematologica 2011; 96(9): 1302–1309
18. Wieckowski EU, Visus C, Szajnik M, Szczepanski MJ, Storkus WJ, Whiteside TL. Tumor-derived microvesicles promote regulatory T cell expansion and induce apoptosis in tumor-reactive activated $CD8^+$ T lymphocytes. J Immunol 2009; 183(6): 3720–3730
19. Hao Q, Wu Y, Wu Y, Wang P, Vadgama JV. Tumor-derived exosomes in tumor-induced immune suppression. Int J Mol Sci 2022; 23(3): 1461
20. Chen Z, You L, Wang L, Huang X, Liu H, Wei JY, Zhu L, Qian W. Dual effect of DLBCL-derived EXOs in lymphoma to improve DC vaccine efficacy *in vitro* while favor tumorgenesis *in vivo*. J Exp Clin Cancer Res 2018; 37(1): 190
21. Hao Y, Chen P, Zhang X, Shao Y, Xu Y, Qian W. The effects of tumor-derived exosomes on T-cell function and efficacy of cancer immunotherapy. ImmunoMedicine 2021; 1(2): e1029
22. Poggio M, Hu T, Pai CC, Chu B, Belair CD, Chang A, Montabana E, Lang UE, Fu Q, Fong L, Blelloch R. Suppression of exosomal PD-L1 induces systemic anti-tumor immunity and memory. Cell 2019; 177(2): 414–427.e13
23. Stüber T, Monjezi R, Wallstabe L, Kühnemundt J, Nietzer SL, Dandekar G, Wöckel A, Einsele H, Wischhusen J, Hudecek M. Inhibition of TGF-β-receptor signaling augments the antitumor function of ROR1-specific CAR T-cells against triple-negative breast cancer. J Immunother Cancer 2020; 8(1): e000676
24. Aung T, Chapuy B, Vogel D, Wenzel D, Oppermann M, Lahmann M, Weinhage T, Menck K, Hupfeld T, Koch R, Trümper L, Wulf GG. Exosomal evasion of humoral immunotherapy in aggressive B-cell lymphoma modulated by ATP-binding cassette transporter A3. Proc Natl Acad Sci USA 2011; 108(37): 15336–15341
25. Aitamer M, Akil H, Vignoles C, Branchaud M, Abraham J, Gachard N, Feuillard J, Jauberteau MO, Shirvani H, Troutaud D, Bentayeb H. CD20 expression, TrkB activation and functional activity of diffuse large B cell lymphoma-derived small extracellular vesicles. Br J Cancer 2021; 125(12): 1687–1698
26. Cox MJ, Lucien F, Sakemura R, Boysen JC, Kim Y, Horvei P, Manriquez Roman C, Hansen MJ, Tapper EE, Siegler EL, Forsman C, Crotts SB, Schick KJ, Hefazi M, Ruff MW, Can I, Adada M, Bezerra E, Kankeu Fonkoua LA, Nevala WK, Braggio E, Ding W, Parikh SA, Kay NE, Kenderian SS. Leukemic extracellular vesicles induce chimeric antigen receptor T cell dysfunction in chronic lymphocytic leukemia. Mol Ther 2021; 29(4): 1529–1540
27. Xhangolli I, Dura B, Lee G, Kim D, Xiao Y, Fan R. Single-cell analysis of CAR-T cell activation reveals a mixed TH1/TH2 response independent of differentiation. Genom Proteom Bioinf 2019; 17(2): 129–139
28. Nakamura K, Kitani A, Strober W. Cell contact-dependent immunosuppression by $CD4^+CD25^+$ regulatory T cells is mediated by cell surface-bound transforming growth factor beta. J Exp Med 2001; 194(5): 629–644
29. Huber S, Schramm C, Lehr HA, Mann A, Schmitt S, Becker C, Protschka M, Galle PR, Neurath MF, Blessing M. TGF-beta signaling is required for the *in vivo* expansion and immunosuppressive capacity of regulatory $CD4^+CD25^+$ T cells. J Immunol 2004; 173(11): 6526–6531
30. Tang N, Cheng C, Zhang X, Qiao M, Li N, Mu W, Wei XF, Han W, Wang H. TGF-β inhibition via CRISPR promotes the long-term efficacy of CAR T cells against solid tumors. JCI Insight 2020; 5(4): e133977
31. Chen W, Konkel JE. TGF-beta and 'adaptive' $Foxp3^+$ regulatory T cells. J Mol Cell Biol 2010; 2(1): 30–36
32. Tone Y, Furuuchi K, Kojima Y, Tykocinski ML, Greene MI, Tone M. Smad3 and NFAT cooperate to induce Foxp3 expression through its enhancer. Nat Immunol 2008; 9(2): 194–202

33. Park BV, Freeman ZT, Ghasemzadeh A, Chattergoon MA, Rutebemberwa A, Steigner J, Winter ME, Huynh TV, Sebald SM, Lee SJ, Pan F, Pardoll DM, Cox AL. TGFβ1-mediated smad3 enhances pd-1 expression on antigen-specific t cells in cancer. Cancer Discov 2016; 6(12): 1366–1381
34. Oksvold MP, Kullmann A, Forfang L, Kierulf B, Li M, Brech A, Vlassov AV, Smeland EB, Neurauter A, Pedersen KW. Expression of B-cell surface antigens in subpopulations of exosomes released from B-cell lymphoma cells. Clin Ther 2014; 36(6): 847–862.e1
35. Ali S, Toews K, Schwiebert S, Klaus A, Winkler A, Grunewald L, Oevermann L, Deubzer HE, Tüns A, Jensen MC, Henssen AG, Eggert A, Schulte JH, Schwich E, Rebmann V, Schramm A, Künkele A. Tumor-derived extracellular vesicles impair cd171-specific $cd4^+$ car t cell efficacy. Front Immunol 2020; 11: 531
36. Lin SC, Haga K, Zeng XL, Estes MK. Generation of CRISPR-Cas9-mediated genetic knockout human intestinal tissue-derived enteroid lines by lentivirus transduction and single-cell cloning. Nat Protoc 2022; 17(4): 1004–1027
37. Tantalo DG, Oliver AJ, von Scheidt B, Harrison AJ, Mueller SN, Kershaw MH, Slaney CY. Understanding T cell phenotype for the design of effective chimeric antigen receptor T cell therapies. J Immunother Cancer 2021; 9(5): e002555
38. Fraietta JA, Lacey SF, Orlando EJ, Pruteanu-Malinici I, Gohil M, Lundh S, Boesteanu AC, Wang Y, O'Connor RS, Hwang WT, Pequignot E, Ambrose DE, Zhang C, Wilcox N, Bedoya F, Dorfmeier C, Chen F, Tian L, Parakandi H, Gupta M, Young RM, Johnson FB, Kulikovskaya I, Liu L, Xu J, Kassim SH, Davis MM, Levine BL, Frey NV, Siegel DL, Huang AC, Wherry EJ, Bitter H, Brogdon JL, Porter DL, June CH, Melenhorst JJ. Determinants of response and resistance to CD19 chimeric antigen receptor (CAR) T cell therapy of chronic lymphocytic leukemia. Nat Med 2018; 24(5): 563–571
39. Chen GM, Chen C, Das RK, Gao P, Chen CH, Bandyopadhyay S, Ding YY, Uzun Y, Yu W, Zhu Q, Myers RM, Grupp SA, Barrett DM, Tan K. Integrative bulk and single-cell profiling of premanufacture t-cell populations reveals factors mediating long-term persistence of CAR T-cell therapy. Cancer Discov 2021; 11(9): 2186–2199
40. Yang C, Kim SH, Bianco NR, Robbins PD. Tumor-derived exosomes confer antigen-specific immunosuppression in a murine delayed-type hypersensitivity model. PLoS One 2011; 6(8): e22517
41. Kloss CC, Lee J, Zhang A, Chen F, Melenhorst JJ, Lacey SF, Maus MV, Fraietta JA, Zhao Y, June CH. Dominant-negative tgf-β receptor enhances psma-targeted human car t cell proliferation and augments prostate cancer eradication. Mol Ther 2018; 26(7): 1855–1866
42. Chen X, Yang S, Li S, Qu Y, Wang HY, Liu J, Dunn ZS, Cinay GE, MacMullan MA, Hu F, Zhang X, Wang P. Secretion of bispecific protein of anti-PD-1 fused with TGF-β trap enhances antitumor efficacy of CAR-T cell therapy. Mol Ther Oncolytics 2021; 21: 144–157
43. Proff J, Brey CU, Ensser A, Holter W, Lehner M. Turning the tables on cytomegalovirus: targeting viral Fc receptors by CARs containing mutated CH2-CH3 IgG spacer domains. J Transl Med 2018; 16(1): 26
44. Boyiadzis M, Whiteside TL. Plasma-derived exosomes in acute myeloid leukemia for detection of minimal residual disease: are we ready? Expert Rev Mol Diagn 2016; 16(6): 623–629